Structure and Ferromagnetism of the Rare-Earth Zintl Compounds: $Yb_{14}MnSb_{11}$ and $Yb_{14}MnBi_{11}$

Julia Y. Chan, Marilyn M. Olmstead, and Susan M. Kauzlarich*

Department of Chemistry, One Shields Avenue, University of California, Davis, California 95616

David J. Webb*

Department of Physics, One Shields Avenue, University of California, Davis, California 95616

Received May 20, 1998. Revised Manuscript Received August 3, 1998

Rare-earth transition metal compounds $Yb_{14}MnSb_{11}$ and $Yb_{14}MnBi_{11}$ have been prepared by heating stoichiometric amounts of the elements at 1000−1200 °C. These compounds are isostructural with the Zintl compound $Ca_{14}AlSb_{11}$ and crystallize in the tetragonal space group $I4_1/acd$ ($Z = 8$). Single-crystal X-ray data (143 K) were refined for $Yb_{14}MnSb_{11}$ [$a =$ 16.615(2) Å, $c = 21.948(4)$ Å, $V = 6059(2)$ Å^3, and $R1/wR2$ (0.0299/0.0479)] and $Yb_{14}MnBi_{11}$ [$a = 17.000(3)$ Å, $c = 22.259(6)$ Å, $V = 6433(2)$ Å^3, $R1/wR2$ (0.0631/0.133)]. Structural analysis is consistent with Yb^{2+}. Temperature-dependent magnetic susceptibility data show that $Yb_{14}MnSb_{11}$ orders ferromagnetically at 56 K and $Yb_{14}MnBi_{11}$ has a ferromagnetic transition at 58 K and another transition at 28 K. High-temperature magnetic susceptibility data can be fit with a modified Curie−Weiss law and give $\mu_{eff} = 4.92(2)\mu_B$ and $\mu_{eff} = 4.9(1)\mu_B$ for the Sb and Bi compounds, respectively. This result is consistent with the assignment of Mn^{3+} (d^4) and Yb^{2+} (f^{14}). Single-crystal magnetic data provide additional evidence for the magnetic transitions and show that the compounds are magnetically anisotropic.

Introduction

Various magnetic behavior has been observed in the $A_{14}MnPn_{11}$ (A = Ca, Sr, Ba; Pn = As, Sb, Bi) compounds.[1] Of the alkaline-earth analogues reported to date, $Ca_{14}MnSb_{11}$ shows the highest temperature ferromagnetic transition of 65 K.[2] The high-temperature magnetic susceptibility is consistent with high spin Mn^{III}, a d^4 ion. The magnetic ordering in the alkaline-earth compounds has been suggested to be of the RKKY (Ruderman-Kittel-Kasuya-Yosida) type, which is the indirect exchange of the localized moments on the Mn mediated by conduction electrons.[2] In the $Eu_{14}MnPn_{11}$ (Pn = Sb, Bi) analogues, where the divalent Eu cations occupy the alkaline-earth sites, a ferromagnetic transition near 100 K is observed for $Eu_{14}MnSb_{11}$.[3] $Eu_{14}MnBi_{11}$ shows an antiferromagnetic behavior at 35 K.[3] The preparation of these rare-earth manganese pnictides has been further motivated by the recent discovery of negative colossal magnetoresistive (CMR) effects in $Eu_{14}MnPn_{11}$ (Pn = Sb, Bi).[4,5] CMR has been observed in single crystals of $Eu_{14}MnSb_{11}$, with MR ratios up to −36% (5 T) near the ferromagnetic transition at 92 K and up to −70% (5 T) for $Eu_{14}MnBi_{11}$ near the antiferromagnetic transition at $T_N \sim 35$ K. The single-crystal magnetoresistance for $Eu_{14}MnBi_{11}$ is large and negative at all temperatures below about 3 T_N. The Yb analogues of this structure type were prepared with the aim of examining the effects of a lanthanide ion without unpaired *f* electrons on the magnetic properties. In this study, the structure and magnetic properties of $Yb_{14}MnPn_{11}$ (Pn = Sb, Bi) will be compared with those of the Ca- and Eu-substituted compounds.

Experimental Section

Synthesis. Dendritic Yb metal (J. Matthey, 99.999%) was cut into small pieces; Sb (J. Matthey, 99.9999%) was used as received; Bi needles (Anderson Physics, 99.999%) were ground into powder; Mn flakes (J. Matthey, 99.98%) were first cleaned in a 5% HNO_3/CH_3OH solution, then transferred into a drybox and ground into a powder. All materials were handled in an argon drybox. Both of the $Yb_{14}MnPn_{11}$ (Pn = Sb, Bi) phases were prepared by enclosing stoichiometric amounts of the elements in welded tantalum (Ta) tubes that were first cleaned with 20% HF, 25% HNO_3, and 55% H_2SO_4 solution. The sealed Ta tube was further sealed in a fused silica tube under 1/5 atm purified argon. High yields of reflective polycrystalline pieces and single-crystal needles were obtained by heating the mixtures to 1000−1200 °C for 5−10 days and cooling the reaction to room temperature at a rate of 60 °C/h. Some reactions were simply quenched to room temperature by turning off the furnace. There are no differences observed between the product from quench versus ramp-cooled reactions. High yield of the $Yb_{14}MnSb_{11}$ and $Yb_{14}MnBi_{11}$ samples could be obtained; however, small amounts of Yb_4Sb_3[6] (for Yb_{14}-

* To whom correspondence should be addressed.

(1) Kauzlarich, S. M. In *Chemistry, Structure, and Bonding of Zintl Phases and Ions*; Kauzlarich, S. M., Ed.; VCH: New York, 1996; p 245.

(2) Rehr, A.; Kuromoto, T. Y.; Kauzlarich, S. M.; Del Castillo, J.; Webb, D. J. *Chem. Mater.* **1994**, *6*, 93.

(3) Chan, J. Y.; Wang, M. E.; Rehr, A.; Kauzlarich, S. M.; Webb, D. J. *Chem. Mater.* **1997**, *9*, 2131.

(4) Chan, J. Y.; Kauzlarich, S. M.; Klavins, P.; Shelton, R. N.; Webb, D. J. *Chem. Mater.* **1997**, *9*, 3132.

(5) Chan, J. Y.; Kauzarich, S. M.; Klavins, P.; Shelton, R. N.; Webb, D. J. *Phys. Rev. B* **1998**, *57*, R8103.

(6) Bodnar, R. E.; Steinfink, H. *Inorg. Chem.* **1967**, *6*, 327.

10.1021/cm980358i CCC: $15.00
Published on Web 10/17/1998

Table 1. Data Collection Paramaters and Crystallographic Data for $Yb_{14}MnSb_{11}$ and $Yb_{14}MnBi_{11}$

parameter	$Yb_{14}MnSb_{11}$	$Yb_{14}MnBi_{11}$
crystal dimens (mm)	0.02 × 0.02 × 0.2	0.11 × 0.18 × 0.28
space group	$I4_1/acd$	$I4_1/acd$
Z	8	8
temp (K)	143	143
lattice params (Å)[a]	$a = 16.615(2)$ $c = 21.948(4)$	$a = 17.000(3)$ $c = 22.259(6)$
cell volume (Å^3)	$V = 6059(2)$	$V = 6433\ (3)$
θ range	$0° < 2\theta < 55°$	$0° < 2\theta < 50°$
scan range (ω) (deg)	0.8	0.8
scan speed (min^{-1})	4.0	4.0
no. of collected reflns	6669	1111
no. of unique reflns	1743	753
no. of params refined	62	62
max and min trans coeff	0.339 and 0.262	0.35 and 0.27
ρ_{calcd} (g cm^{-3})	8.368	9.863
μ Mo Kα (mm^{-1})	52.711	100.512
$R1$ [$I > 2\sigma(I)$][b]	0.0299	0.0631
$wR2$[c]	0.0479	0.1335
largest diff peak and hole (e Å^{-3})	1.706 and −1.807	4.443 and −3.714

[a] Room temperature lattice parameters obtained from Guinier powder diffraction are $a = 16.621(6)$ Å, $c = 21.91(2)$ Å ($Yb_{14}MnSb_{11}$) and $a = 17.024(8)$ Å, $c = 22.26(4)$ Å ($Yb_{14}MnBi_{11}$). [b] $R = \sum||F_o| - |F_c||/\sum|F_o|$. [c] $wR2 = \sum[w(F_o^2 - F_c^2)^2]/\sum[w(F_o^2)^2]^{1/2}$.

$MnSb_{11}$) and Yb_5Bi_3[7] (for $Yb_{14}MnBi_{11}$) were identified as an impurity in the reactions that were heated at temperatures <1100 °C. The best method to date for producing crystals from the elements was in a 2-zone furnace with $T_{high} = 1100$ °C and $T_{low} = 1050$ °C for 10 days. All reactions were opened and examined in a nitrogen-filled drybox equipped with a microscope with water levels <1 ppm. Both compounds are air and water sensitive.

X-ray Powder Diffraction. The products were examined in a drybox, under an atmosphere of N_2, mixed with approximately 10% silicon and placed between two pieces of cellophane tape. The sample was then transferred to an Enraf Nonius Guinier camera utilizing CuKα_1 radiation. Powder diffraction patterns were compared with those calculated from crystal structure data using the program POWDER.[8] Diffraction line positions were read and 2θ values, d spacings, and error bars were obtained from the program GUIN.[9] The 2θ values were indexed and lattice parameters were refined using the program LATT.[10] The room-temperature lattice parameters are provided in Table 1.

Single-Crystal X-ray Diffraction. The Ta tube was opened in a drybox equipped with a microscope. Needle-shaped, highly reflective crystals were transferred to Exxon Paratone N oil for X-ray structure determination. A suitable crystal (0.02 × 0.02 × 0.2 mm for $Yb_{14}MnSb_{11}$) and (0.11 × 0.18 × 0.28 mm for $Yb_{14}MnBi_{11}$) was mounted on a thin glass fiber and was positioned under a cold stream of N_2 (143 K) in a $R3m/V$ Siemens Diffractometer with a modified Enraf-Nonius low-temperature apparatus (Mo Kα, $\lambda = 0.71069$ Å) and a graphite monochromator. Data collection parameters and crystallographic data are provided in Table 1. The lattice parameters were verified from axial photographs. No decomposition of the crystal was observed (inferred from the intensity of the two check reflections). A Ψ scan empirical absorption correction was performed for the $Yb_{14}MnSb_{11}$ compound. The structures were solved by direct methods and were refined using SHELXTL Version 5.03.[11] The $Yb_{14}MnBi_{11}$ data were corrected for absorption[12,13] after the refinement converged with isotropic Us, and all the atoms were then refined with anisotropic Us. Largest features in the final difference map for $Yb_{14}MnSb_{11}$ are 1.71 e$^-$/Å^3 and −1.81 e$^-$/Å^3. The statistics for the $Yb_{14}MnBi_{11}$ structure are not as good as for the Sb compound because of the smaller data set collected. Because the Bi compound is isostructural to the Sb compound and there were no anomalies with respect to the structure or the refinement, this data set was deemed sufficient. No additional crystals were examined. Atomic coordinates and isotropic thermal parameters are provided in Table 2. Detailed data collection parameters, crystallographic data, and anisotropic thermal parameters are provided as Supporting Information.

Table 2. Atomic Coordinates [×10^4] and Equivalent Isotropic Displacement Parameters [Å^2 × 10^3] for $Yb_{14}MnSb_{11}$ and $Yb_{14}MnBi_{11}$

atom	x	y	z	U(eq)[a]
		$Yb_{14}MnSb_{11}$		
Sb(1)	1360(1)	3860(1)	1250	5(1)
Sb(2)	49(1)	1086(1)	8100(1)	7(1)
Sb(3)	8695(1)	9732(1)	9526(1)	7(1)
Sb(4)	0	2500	1250	7(1)
Yb(1)	−422(1)	−738(1)	8281(1)	7(1)
Yb(2)	−224(1)	1241(1)	28(1)	9(1)
Yb(3)	3550(1)	0	2500	7(1)
Yb(4)	1795(1)	4089(1)	8427(1)	8(1)
Mn(1)	0	2500	8750	7(1)
		$Yb_{14}MnBi_{11}$		
Bi(1)	1389(2)	3888(2)	1250	9(1)
Bi(2)	66(2)	1077(2)	8115(1)	13(1)
Bi(3)	8693(2)	9723(2)	9531(1)	12(1)
Bi(4)	0	2500	1250	12(1)
Yb(1)	−405(2)	−747(2)	8281(1)	11(1)
Yb(2)	−229(2)	1232(2)	17(1)	16(1)
Yb(3)	3540(3)	0	2500	13(1)
Yb(4)	1776(2)	4106(2)	8424(1)	14(1)
Mn(1)	0	2500	8750	18(5)

[a] U(eq) is defined as one-third of the trace of the orthogonalized $U(ij)$ tensor.

Magnetic Susceptibility Measurements. Direct current (dc) magnetization data were obtained with a Quantum Design MPMS Superconducting Quantum Interference Device (SQUID) magnetometer with a 5.5 T superconducting magnet. The data were collected and analyzed with the Magnetic Property Measurement System (MPMS) software supplied by Quantum Design.[14] The samples were prepared in a drybox, typically by loading 20−25 mg of powdered sample into a quartz tube designed to provide minimal, uniform background. The tube was subsequently sealed under vacuum (1×10^{-6} Torr). For single-crystal magnetic measurements, a single needle (0.5−1.0 mm) was placed in a straw fixed with Apiezon grease type N. The c-axis of the needle was subsequently turned 90° for measurement of the field perpendicular to the applied magnetic field. The temperature-dependent magnetization data were obtained by first measuring the zero field-cooled (ZFC) magnetization in the field while warming from 5 to 300 K, then measuring magnetization while cooling back to 5 K with the field applied to obtain the field-cooled (FC) data. Field-dependent magnetization data were taken at 5 K with the field, H, swept from 0 to 5 T, to −5 T, and back to 0 T. The applied H is 1000 Oe for single-crystal measurements and 500 Oe for bulk samples. The larger field was necessary for the single crystals to achieve adequate signal-to-noise in the

(7) Leon-Escamilla, E. A.; Corbett, J. D. *J. Alloys Compd.* **1994**, *206*, L15.
(8) Clark, C. M.; Smith, D. K.; Johnson, G. J. *POWDER, FORTRAN IV program for calculating X-ray diffraction patterns*; Department of Geosciences, Pennsylvania State University, University Park, PA, 1973; Version 5.
(9) Imoto, H. *GUIN, Fortran Program to calculate 2-theta from film with Si reference lines*; Iowa State University, 1979.
(10) Lii, K.; Wang, S.; Garcia, E. *LATT*; Iowa State University, 1985.
(11) Sheldrick, G. M. *SHELXTL, A Program for Crystal Structure Determination*; Madison, Wisconsin, Siemens Analytical X-ray Instruments, 1994, 5.03.
(12) Hope, H.; Moezzi, B., *Program XABS2*, Chemistry Department, University of California, Davis, CA, 1995.
(13) Parkin, S.; Moezzi, B.; Hope, H. *J. Appl. Crystallogr.* **1995**, *28*, 53.
(14) Quantum Design Inc., San Diego, CA 92121.

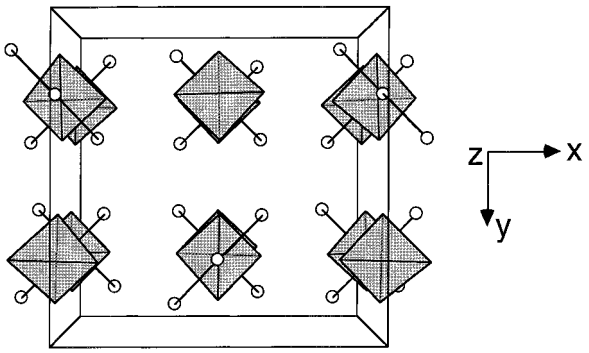

Figure 1. Perspective view down the *c*-axis showing the tetrahedra and the polyatomic Sb_3^{7-} units.

Table 3. Selected Bond Distances (Å) and Angles (deg)

bond	$Yb_{14}MnSb_{11}$	$Yb_{14}MnBi_{11}$
Pn(1)−Pn(4)	3.195(1)	3.336(1)
Pn(1)−Yb(1) × 2	3.204(1)	3.280(1)
Pn(1)−Yb(2) × 2	3.284(1)	3.383(1)
Pn(1)−Yb(3)	3.338(1)	3.363(1)
Pn(1)−Yb(4)	3.171(1)	3.222(1)
Pn(2)−Mn × 4	2.750(1)	2.803(1)
Pn(2)−Yb(1)	3.155(1)	3.218(1)
Pn(2)−Yb(1′)	3.180(1)	3.255(1)
Pn(2)−Yb(2)	3.745(1)	3.872(1)
Pn(2)−Yb(2′)	3.139(1)	3.205(1)
Pn(2)−Yb(3)	3.226(1)	3.290(1)
Pn(2)−Yb(4)	3.159(1)	3.219(1)
Pn(2)−Yb(4′)	3.394(1)	3.433(1)
Pn(3)−Yb(1)	3.175(1)	3.274(1)
Pn(3)−Yb(1′)	3.194(1)	3.254(1)
Pn(3)−Yb(2)	3.167(1)	3.330(1)
Pn(3)−Yb(2′)	3.274(1)	3.234(1)
Pn(3)−Yb(3)	3.134(1)	3.194(1)
Pn(3)−Yb(4)	3.212(1)	3.264(1)
Pn(3)−Yb(4′)	3.194(1)	3.230(1)
Pn(3)−Yb(4″)	3.709(1)	3.765(1)
Pn(4)−Yb(1) × 4	3.181(1)	3.230(1)
Pn(4)−Yb(2) × 4	3.423(1)	3.511(1)
Pn(2)−M−Pn(2′)	105.61(2)	104.72(5)
Pn(2)−M−Pn(2″)	117.50(4)	119.4(1)
Mn···Mn	9.954(1)	10.155(1)

paramagnetic regime. Several crystals of each compound were measured and provide reproducible results.

Results and Discussion

Structure. Data collection parameters for $Yb_{14}MnSb_{11}$ and $Yb_{14}MnBi_{11}$ are shown in Table 1. Positional parameters along with isotropic thermal parameters are provided in Table 2. Table 3 presents selected bond distances for $Yb_{14}MnSb_{11}$ and $Yb_{14}MnBi_{11}$. All compounds are isostructural to $Ca_{14}AlSb_{11}$,[15] which has been described in detail previously.[1−3,16,17] The structure can be described as containing 14 Yb^{2+} cations, a $MnPn_4^{9-}$ tetrahedron, a Pn_3^{7-} polyatomic anion, and 4 Pn^{3-} anions. Figure 1 shows a view of the structure with only the $MnPn_4$ tetrahedra and the linear polyatomic linear Pn_3^{7-} anions. The Pn_3^{7-} anion is best described as a hypervalent 3*c*−4*e* bond, isoelectronic to the I_3^- anion.[18] The tetrahedra are stacked and translated by 1/2 along the *c*-axis, alternated by the Sb_3 or Bi_3 polyatomic anions.

The Yb analogues will be compared with the Ca compounds because the ionic radii of Ca^{2+} and Yb^{2+} are almost the same (Yb^{2+} has an ionic radius of 1.02 Å and Ca^{2+} has an ionic radius of 1.00 Å).[19] Therefore, we can compare the distances and angles to provide some insight into the bonding and the resulting magnetic properties.

The $MnSb_4$ tetrahedron is more distorted for the Yb than the Ca compound, with angles of 106.6(1)° and 115.3(1)° for the Ca compound and 105.61(2)° and 117.50(4)° for $Yb_{14}MnSb_{11}$. A similar magnitude of distortion is also observed in the Eu analogues,[3] where the tetrahedron is more distorted than the similarly sized Sr compound.[2] The Mn−Sb(2) distances are quite comparable at 2.759(2) Å and 2.750(1) Å for the Ca and Yb compounds, respectively. The $MnBi_4$ tetrahedron in $Yb_{14}MnBi_{11}$ is also more distorted than that in the corresponding Ca compound with 105.4(1)° and 118.0(1)° for $Ca_{14}MnBi_{11}$[16] and 104.72(5)° and 119.4(1)° for the Yb compound. The Mn−Bi(2) distances are comparable at 2.803(1) Å and 2.814(1) Å for the Yb and Ca compounds, respectively.

The Sb−Sb distances in the linear chain are slightly shorter for the Yb compound, with Ca and Yb having distances of 3.215(2) and 3.195(1) Å, respectively; a similar trend is also observed in the Eu analogues. The Bi−Bi distances in the linear chain are comparable, with distances of 3.336(1) and 3.335(1) Å for the Ca and Yb compounds, respectively. The Pn−Pn distances are comparable to those in the $Ca_{11}Pn_{10}$ phase, where Pn−Pn distances range from 2.95 to 3.36 Å and 3.15 to 3.34 Å for the Sb and Bi compounds, respectively.[20] These long distances have been discussed in detail and are consistent with the interpretation of a hypervalent species.[18]

The Yb−Sb bond distances in $Yb_{14}MnSb_{11}$ range from 3.155(1) Å for Yb(1)−Sb(2) to 3.394(1) Å for Yb(4)−Sb(2). The A(3)−Sb(2) (A = Yb, Ca) distances are shorter for the Yb compound [3.227(1) Å] than for $Ca_{14}MnSb_{11}$ [3.403(4) Å].[2] In the β-structure of Yb_5Sb_3, Yb−Sb distances range from 3.044 to 3.543 Å.[21] In the metallic $YbSb_2$ phase, Yb−Sb distances range from 3.193(10) to 3.570(10) Å.[22] The longest Yb−Sb distance of 3.745(1) Å is significantly larger, and is not considered a bonding interaction. The A−Bi (A = Yb, Ca) distances in $Yb_{14}MnBi_{11}$ are similar to those in the Ca analogue, with Yb−Bi bond distances ranging from 3.194(1) to 3.433(1) Å and Ca−Bi distances ranging from 3.201(1) to 3.453(1) Å.[16] The longest Yb−Bi distance observed is 3.872(1) Å and is not considered a bonding interaction. The bond distances observed are consistent with other Yb^{2+}-containing compounds and the proposed Yb^{2+} oxidation state.

Magnetism. Figure 2 shows the temperature-dependent magnetic susceptibility of $Yb_{14}MnSb_{11}$ at 500 Oe. The inset shows the reciprocal magnetic susceptibility as a function of temperature. High-temperature

(15) Cordier, G.; Schäfer, H.; Stelter, M. *Z. Anorg. Allg. Chem.* **1984**, *519*, 183.
(16) Kuromoto, T. Y.; Kauzlarich, S. M.; Webb, D. J. *Chem. Mater.* **1992**, *4*, 435.
(17) Rehr, A.; Kauzlarich, S. M. *J. Alloys Compd.* **1994**, *207/208*, 424.
(18) Gallup, R. F.; Fong, C. Y.; Kauzlarich, S. M. *Inorg. Chem.* **1992**, *31*, 115.
(19) Shannon, R. D. *Acta Crystallogr.* **1976**, *A32*, 751.
(20) Deller, K.; Eisenmann, B. *Z. Naturforsch* **1976**, *31b*, 29.
(21) Brunton, G. D.; Steinfink, H. *Inorg. Chem.* **1971**, *10*, 2301.
(22) Wang, R.; Bodnar, R.; Steinfink, H. *Inorg. Chem.* **1966**, *5*, 1468.

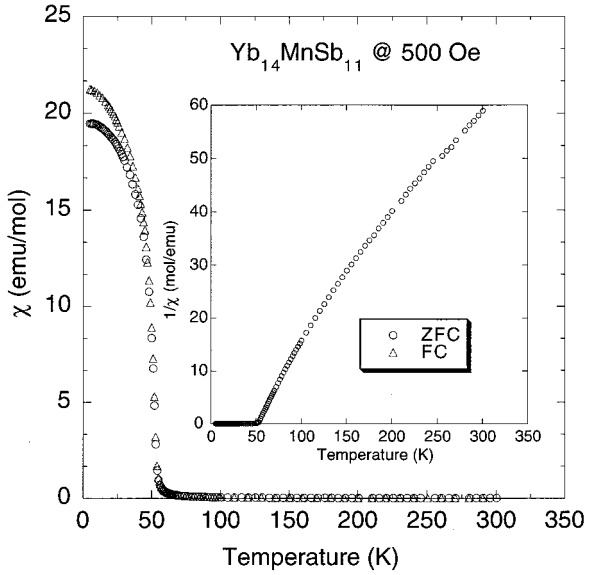

Figure 2. Temperature-dependent magnetic susceptibility of $Yb_{14}MnSb_{11}$ at 500 Oe. Zero field-cooled (ZFC) and field-cooled (FC) data are shown.

Table 4. Magnetic Properties of $Yb_{14}MnPn_{11}$ (Pn = Sb, Bi)

property	$Yb_{14}MnSb_{11}$	$Yb_{14}MnBi_{11}$
χ_o (emu/mol)[a]	0.00502(9)	0.001(2)
C[a]	3.04(2)	3.1(4)
θ (K)[a]	48.0(1)	50.5(5)
μ_{eff} (μ_B)[b]	4.92(2)	4.9(1)
T_c (K)	56	60/28
fit range (K)	105−300	100−300

[a] Obtained from fitting the data to equation $\chi = \chi_o + C/(T - \theta)$. [b] Using the equation $\mu_{eff} = (7.99\ C)^{1/2}$.

data can be fit to the Curie−Weiss law plus a temperature-independent parameter, χ_o. Table 4 shows the fits obtained from the magnetic data of powder samples of $Yb_{14}MnSb_{11}$ and $Yb_{14}MnBi_{11}$. The magnetic constants [$\chi_o = 0.00502(9)$ emu/mol, $C = 3.04(2)$, and $\theta = 48.0(1)$ K] were obtained from fitting the data to a modified Curie−Weiss formula $\chi = \chi_o + C/(T - \theta)$. The effective moment, μ_{eff}, of $4.92(2)\mu_B$, is obtained from the equation $\mu_{eff} = \sqrt{7.99C}$ and is consistent with the spin-only value of $4.9\mu_B$ for Mn^{3+} (d^4). The observed transition temperature (T_c) of 56 K is lower than that of the $Ca_{14}MnSb_{11}$ compound, which has a T_c of 65 K.[2] Figure 3 shows a hysteresis loop at 5 K. The saturation moment at 5 T is close to $6.6\mu_B$. Because the only magnetic ion in $Yb_{14}MnSb_{11}$ are Mn^{3+} ions, one would expect a saturation moment of $4\mu_B$ consistent with the spin-only value associated with four unpaired spins. A moment $>4\mu_B$ suggests that other magnetic ions are present and it is possible that some of the Yb is present as Yb^{3+}. To explore this hypothesis, field-dependent magnetization at 5, 30, and 56 K was measured, and the results are shown in Figure 4. At 56 K and 5 T, the magnetic ordering temperature, the moment is approximately $4\mu_B$. However, below T_c, at 30 and 5 K (5 T), a saturation moments of $6.0\mu_B$ and $6.6\mu_B$, respectively, are observed.

The relationship between atom separation and the observed magnetic moment has been correlated in the Yb−Sb system, where a distance of 3.2 Å corresponds to a divalent Yb.[23] This result is consistent with Yb−Sb distances observed in $Yb_{14}MnSb_{11}$ and suggests that all the Yb in this compound is present as Yb^{2+}. The high-temperature magnetic data (105−300 K) of $Yb_{14}MnSb_{11}$ are consistent with 14 Yb^{2+} cations (nonmagnetic), with the moment μ_{eff} consistent with Mn^{3+}, high-spin d^4, similar to other compounds of this structure type. However, below the ferromagnetic ordering temperature of 56 K, the saturation moment increases from $\mu_{sat} = 4.0\mu_B$ to $\mu_{sat} = 6.6\mu_B$ at 5 K at 5 T. Because $Yb_{14}MnSb_{11}$ is isostructural to the Zintl phase, $Ca_{14}AlSb_{11}$, mixed valency of Yb seems unlikely. Small amounts of a Yb^{3+} phase could contribute to the saturation moment at low temperature. The additional $2.6\mu_B$ observed at 5 K corresponds to a fraction of 2.6/4.54 Yb^{3+} ($p = 4.54\mu_B$ for Yb^{3+}) moment. This result is consistent with approximately 4% Yb^{3+} impurity, which is less than the detection limit in powder X-ray diffraction. The most likely impurities are Yb_4Sb_3[6] (for $Yb_{14}MnSb_{11}$) and Yb_5Bi_3[7] (for $Yb_{14}MnBi_{11}$), which were sometimes observed

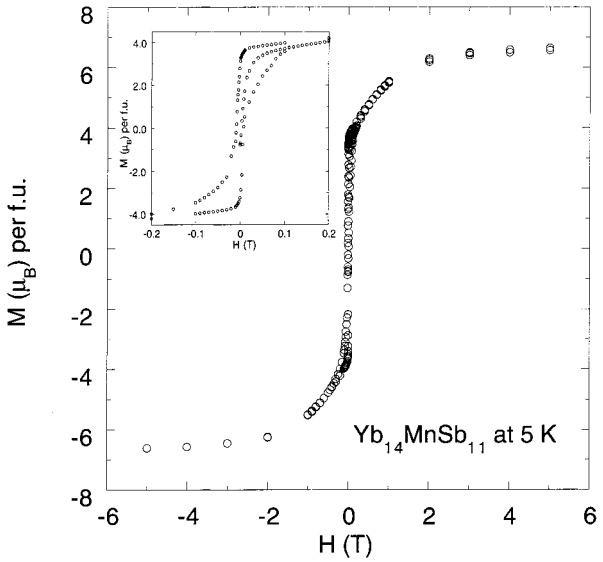

Figure 3. Hysteresis loop of $Yb_{14}MnSb_{11}$ at 5 K.

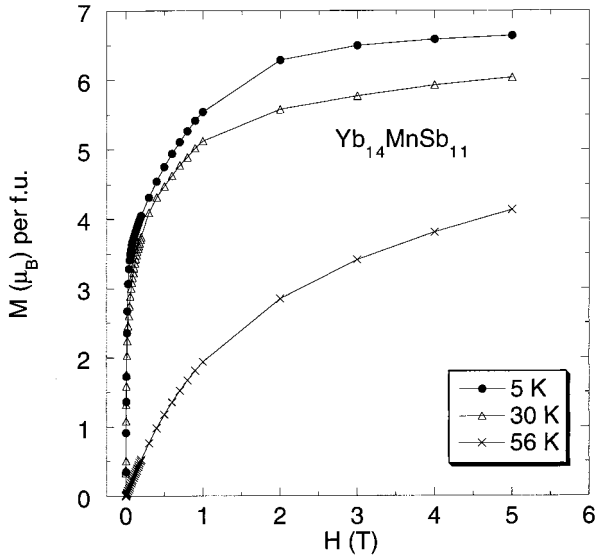

Figure 4. Field-dependent magnetic susceptibility of $Yb_{14}MnSb_{11}$ at 5, 30, and 56 K.

(23) Bodnar, R. E.; Steinfink, H.; Narasimhan, S. V. L. *J. Appl. Phys.* **1968**, *39*, 1485.

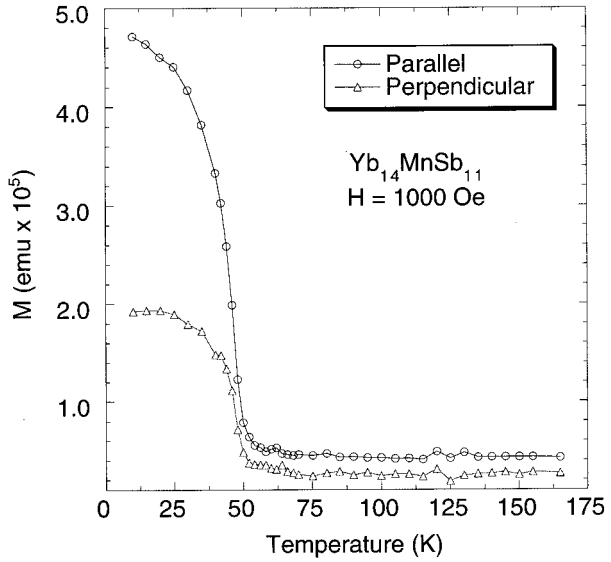

Figure 5. Temperature-dependent magnetization of a single crystal of $Yb_{14}MnSb_{11}$ with the *c*-axis oriented parallel and perpendicular to the applied magnetic field measured at 1000 Oe.

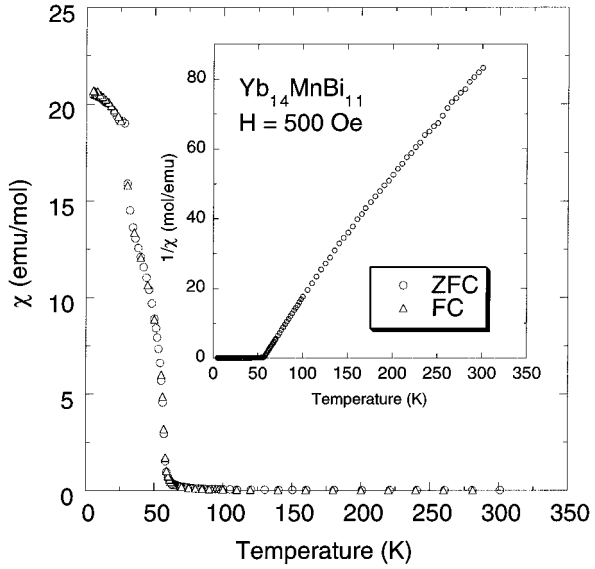

Figure 6. Temperature-dependent magnetic susceptibility of $Yb_{14}MnBi_{11}$ at 500 Oe. Zero field-cooled (ZFC) and field-cooled (FC) data are shown.

in the powder diffraction pattern. The nonlinearity slightly below the saturation moment of the field-dependent magnetization is likely due to the Brillouin function saturation of a minor magnetic impurity containing Yb^{3+}.

Magnetic measurements were made on a single crystal to provide further characterization of this compound. Figure 5 shows the single-crystal temperature-dependent magnetization of a single needle-shaped crystal of $Yb_{14}MnSb_{11}$ parallel and perpendicular to the applied magnetic field measured at 1000 Oe. A transition temperature of 56 K, which is consistent with the bulk magnetic data, is observed. At this magnetic field, the magnetic moment for the crystal oriented in the parallel direction is 2.5 times larger than the moment when oriented perpendicular to the field. This result suggests that, after taking the crystal shape into account, there is a magnetic easy axis along the *c*-axis.

Figure 6 shows the temperature-dependent magnetic susceptibility of $Yb_{14}MnBi_{11}$ polycrystalline sample measured at 500 Oe. The high-temperature magnetic data (100−300 K) could also be fit to the modified Curie−Weiss law and $\chi_o = 0.001(2)$, $C = 3.1(4)$, $\theta = 50.5(5)$ K, and $\mu_{eff} = 4.9(1)$, consistent with a Mn^{3+} d^4 system with nonmagnetic 14 Yb^{2+} cations. There are two transitions observed in the susceptibility data, a ferromagnetic transition of 58 K and a second at the discontinuous point of 28 K. The ferromagnetic transition at 58 K is slightly higher than that observed in $Ca_{14}MnBi_{11}$ ($T_c = 55$ K). However, in both cases, a Weiss constant of 50 K is obtained. The 58 K transition of the $Yb_{14}MnBi_{11}$ can be attributed to the Mn ordering, because the Mn···Mn distances in both compounds are similar at 10.183(3) and 10.155(1) Å for $Ca_{14}MnBi_{11}$ and $Yb_{14}MnBi_{11}$, respectively.

Figure 7 shows the hysteresis loops of $Yb_{14}MnBi_{11}$ of the powder sample at 5, 30, and 58 K. At 5 K, the moment is 5.2μ_B, which is higher than the 4μ_B ordered moment predicted for a d^4 Mn^{3+} system. For the same reasons as already stated for $Yb_{14}MnSb_{11}$, this slight increase in moment is attributed to the presence of a small amount of Yb^{3+} (approximately 2% impurity).

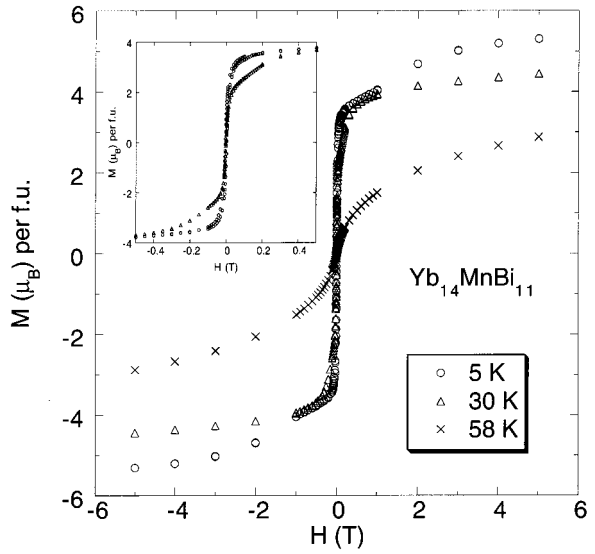

Figure 7. Hysteresis loops of $Yb_{14}MnBi_{11}$ at 5, 30, and 58 K.

Hysteresis loops of the bulk sample of $Yb_{14}MnBi_{11}$ show that at 30 K, the moment at 5 T is 4.0μ_B, and at 58 K, the moment at 5 T is 2.9μ_B.

Because of the presence of the discontinuity at 28 K, magnetization measurements on a single crystal were performed to gain more information concerning the origin of the transition. The two transitions are observed in the single-crystal data with the crystallographic *c*-axis of the unit cell parallel to the applied magnetic field, as shown in Figure 8. Only the transition temperature at 28 K is observed with the *c*-axis perpendicular to the magnetic field. The transition near 60 K is observed for the *c*-axis of the crystal aligned parallel to the field; however, near 30 K, the magnetization drops. The reduction of the moment measured with the *c*-axis parallel is matched by the increase in moment at 30 K for the $Yb_{14}MnBi_{11}$ single-crystal oriented perpendicular to the crystallographic *c*-axis. The low-temperature transition can be attributed to spin reorientation caused by either a structural or electronic transition at 28 K. The reduction of the moment along

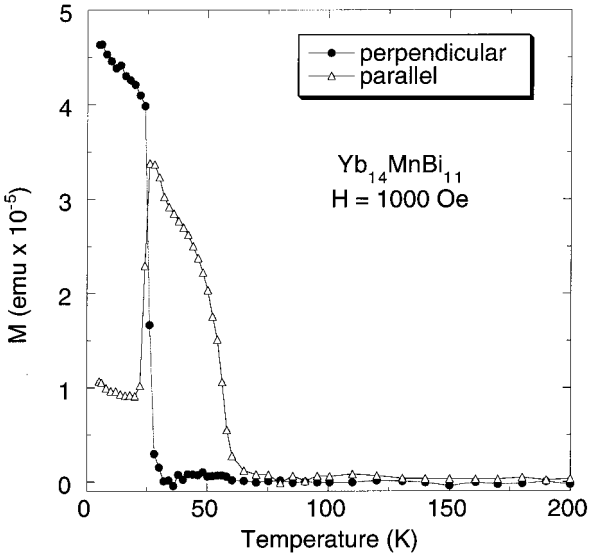

Figure 8. Temperature-dependent magnetization of a single crystal of $Yb_{14}MnBi_{11}$ with the *c*-axis oriented parallel and perpendicular to the applied magnetic field, $H = 1000$ Oe.

the *c*-axis occurs at the same temperature as the increase in moment for the $Yb_{14}MnBi_{11}$ oriented perpendicular to the *c*-axis. However, the reduction in the moment along the *c*-axis is smaller than the increase perpendicular to the *c*-axis. It appears that the moment is rising when measured along the *c*-axis even before the spin direction switches.

We can compare the $Yb_{14}MnPn_{11}$ compounds to the $A_{14}MnPn_{11}$ compounds by comparing the data with the predictions of the RKKY theory of magnetic coupling.[24] The paramagnetic Curie temperature ($\theta = NS(S + 1)A(2k_F)^3F(r)$, where $N =$ number of Mn neighbors, $S = 2$ is the Mn local spins, A is the parameter related to the strength of the interaction between a conduction electron and the local Mn spin, k_F is the Fermi wavevector, and $F(r) = [2k_Fr\cos(k_Fr) - \sin(k_Fr)]/(k_Fr)^4$) has been used to fit the magnetic data of $A_{14}MnPn_{11}$.[2] Because the high-temperature magnetic data indicate that all of the Yb is divalent at high temperatures, this system should follow the RKKY theory. All the parameters obtained from the high-temperature fit agree well with the theory. Figure 9 shows T_c plotted as a function of Mn···Mn distance for all of the $A_{14}MnPn_{11}$ compounds except for A = Eu compound, where there are Eu···Mn and Eu···Eu interactions that may affect θ. The fit corresponds to the parametrization of the data to the free electron isotropic RKKY theory with $k_F = 0.5$ Å^{-1}, which sets the length scale of the interaction, and $A = 1.3 \times 10^{-37}$ erg cm^3. This plot shows that the coupling strength is greater with decreasing distances, and one would expect that the transition temperature for the Sb compound be higher than the Bi compound. However, the Sb compound is anomalous and has a lower ordering temperature than the Bi compound. This result suggests that the second nearest neighbor Mn···Mn interactions and more subtle electronic effects may contribute to the ordering temperature in this class of compounds. Further work is in progress on single crystals to explore the magnetic properties in these compounds.

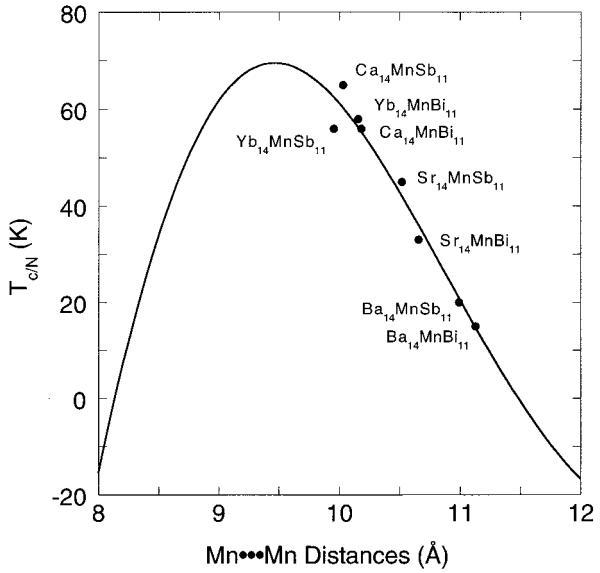

Figure 9. Mean field $T_{c/N}$ as a function of Mn···Mn distance for the $A_{14}MnPn_{11}$ compounds. The solid line represents the parametrization of the data to a simple free electron isotropic RKKY theory with $\theta = NS(S + 1)A(2k_F)^3F(r)$, where $N =$ number of Mn neighbors, $S = 2$ is the Mn local spins, k_F is the Fermi wavevector, $F(r) = [2k_Fr\cos(k_Fr) - \sin(k_Fr)]/(k_Fr)^4$), $k_F = 0.5$ Å^{-1}, and $A = 1.5 \times 10^{-37}$ erg cm^3.

Summary

The bond distances determined from the single-crystal structure are comparable with those of the Ca analogues and consistent with the assignment of Yb^{2+}. The $MnPn_4$ tetrahedron shows a larger distortion than the Ca analogue. A similar effect is seen with Eu when compared with the Sr analogues and suggests that electronic effects rather than matrix effects may be important. Magnetization measurements on bulk samples show an effective moment at high temperatures consistent with Mn^{3+} as the only magnetic ion in these compounds. $Yb_{14}MnSb_{11}$ shows ferromagnetic ordering at 56 K and the saturation moment at that temperature consistent with all the Mn ordering ferromagnetically. The $Yb_{14}MnBi_{11}$ orders ferromagnetically at 58 K with a second transition at 28 K. Single-crystal magnetization data show that the magnetic properties are anisotropic. We suggest that the 28 K transition observed in $Yb_{14}MnBi_{11}$ is due to spin reorientation caused by a structural or electronic transition. The magnetism in these compounds can be qualitatively understood within the RKKY theory. However, more detailed measurements are necessary to understand the relationship between the structure and magnetic properties.

Acknowledgment. We thank P. Klavins for assistance, R. N. Shelton for use of the magnetometer, and P. C. Canfield and I. R. Fisher for useful disscussion. Financial support by the National Science Foundation, Division of Materials Research (DMR-9505565) is gratefully acknowledged.

Supporting Information Available: Additional diffraction and refinement data and anisotropic displacement parameters for $Yb_{14}MnSb_{11}$ and $Yb_{14}MnBi_{11}$ (3 pages). Ordering information is given on any current masthead page.

CM980358I

(24) Liu, L. *Solid State Commun.* **1980**, *35*, 187.